Journal of *Marine Science and Engineering*

MDPI

Article

Sediment Provenance and Facies Analysis of the Huagang Formation in the Y-Area of the Central Anticlinal Zone, Xihu Sag, East China Sea

Xiao Ma [1], Wei Yan [2,*], Yi Yang [1], Ru Sun [1], Yue Chao [1], Guoqing Zhang [2], Chao Yang [1], Shudi Zhang [1], Dapeng Su [3], Guangxue Zhang [2] and Hong Xu [3,4,5,*]

[1] Research Institute of Exploration and Development, Shanghai Offshore Oil and Gas Company, SINOPEC, Shanghai 200120, China; max.shhy@sinopec.com (X.M.)
[2] Guangzhou Marine Geological Survey, Guangzhou 511458, China
[3] Qingdao Institute of Marine Geology, Qingdao 266073, China
[4] First Institute of Oceanography, Ministry of Natural Resources, Qingdao 266061, China
[5] Yangtze University (Wuhan), Wuhan 434100, China
* Correspondence: williambjyw@hotmail.com (W.Y.); qdxhong@163.com (H.X.)

Abstract: Recent breakthrough exploration wells in the Huagang Formation in the Y-area of the central anticlinal zone of the Xihu Sag have confirmed the significant exploration potential of structure–lithology complex hydrocarbon reservoirs. However, limited understanding of the provenance system, sedimentary facies, and microfacies has hindered further progress in complex hydrocarbon exploration. Analysis of high-precision stratigraphic sequences and seismic facies data, mudstone core color, grain-size probability cumulative curves, core facies, well logging facies, lithic type, the heavy-mineral ZTR index, and conglomerate combinations in drilling sands reveals characteristics of the source sink system and provenance direction. The Huagang Formation in the Y-area represents an overall continental fluvial delta sedimentary system that evolved from a braided river delta front deposit into a meandering river channel large-scale river deposit. The results indicate that the primary provenance of the Huagang Formation in the Y-area of the Xihu Sag is the long-axis provenance of the Hupi Reef bulge in the northeast, with supplementary input from the short-axis provenance of the western reef bulge. Geochemical analysis of wells F1, F3, and G in the study area suggests that the prevailing sedimentary environment during the period under investigation was characterized by anoxic conditions in nearshore shallow waters. This confirms previous research indicating strong tectonic reversal in the northeast and a small thickness of the central sand body unrelated to the flank slope provenance system. The aforementioned findings deviate from conventional understanding and will serve as a valuable point of reference for future breakthroughs in exploration.

Keywords: Xihu Sag; Huagang Formation; provenance analysis; sedimentary facies; heavy minerals

check for updates

Academic Editor: Manuel Martín-Martín

Received: 9 January 2025
Revised: 17 February 2025
Accepted: 18 February 2025
Published: 9 March 2025

Citation: Ma, X.; Yan, W.; Yang, Y.; Sun, R.; Chao, Y.; Zhang, G.; Yang, C.; Zhang, S.; Su, D.; Zhang, G.; et al. Sediment Provenance and Facies Analysis of the Huagang Formation in the Y-Area of the Central Anticlinal Zone, Xihu Sag, East China Sea. *J. Mar. Sci. Eng.* **2025**, *13*, 520. https://doi.org/10.3390/jmse13030520

Copyright: © 2025 by the authors. Licensee MDPI, Basel, Switzerland. This article is an open access article distributed under the terms and conditions of the Creative Commons Attribution (CC BY) license (https://creativecommons.org/licenses/by/4.0/).

1. Introduction

The Y-area of the Xihu Sag has a rich exploration history and an intricate exploration process. In 1984, 1993, 2013, and 2014, one exploratory well was drilled in each of the four local structural highs located in the northern, central, and southern parts of the Yuquan Structure, respectively (Figure 1). However, despite these efforts, the overall exploration results were unsatisfactory, as they encountered challenges in unlocking a single gas reservoir within these structural formations. After 2018, leveraging the successful

exploration and development experience of structure–lithology complex reservoirs in other regions of the Xihu Sag, the concept of lithologic reservoir exploration was employed to reevaluate and assess the Y-area. As a result, strategically positioning well E in the lower section of the central structural high point ultimately led to a breakthrough and confirmed this region's potential for composite lithologic–structural trap exploration.

Nearly a decade of research has clarified the diagenetic environment and pore structure changes in tight sandstone reservoirs like the Huagang Formation. Studies have explored the relationship between numerical simulation inversion dynamics and hydrocarbon accumulation, as well as the petrology, mineralogy, and isotope geochemistry of diagenetic fluid evolution in the Granite Formation [1–3]. Burial history analysis has examined the diagenesis and hydrocarbon accumulation characteristics of Huagang Formation sandstone and the impact of clay minerals on reservoir quality [4,5]. Research has also discussed the diagenetic evolution of the Huagang Formation, including the relationship between tight sandstone fractures and hydrocarbon accumulation, and identified controlling factors for tight sandstone reservoir development in the central tectonic inversion belt of the Granite Formation and sedimentary characteristics of large coastal bars [6–8]. Several scholars have studied the structure and lithology of the Huagang Formation, hydrocarbon geochemistry, and gas migration mechanisms in large- and medium-sized oil and gas fields [9–12]. These studies have explored how provenance, clastic composition, and diagenesis affect these formations [13]. Research has also examined tectonic inversion, fault systems, and changes in sedimentary strata within the Huagang Formation [14]. Seismic sedimentology has been used to analyze the fluvial delta reservoir system, revealing structural features and migration mechanisms in the tensile rift zone [15].

However, research addressing the exploration bottlenecks in the Y-area remains inadequate, and the comprehension of sediment-reservoir source–sink systems and composite hydrocarbon reservoirs lacks clarity. There is a lack of fundamental understanding of exploration challenges, such as the determination of source and sedimentary facies characteristics in the central structural belt of the Y-area, the number of sources, and the proportion of each source's contribution in the reservoir. In particular, the understanding of the source–sink system and sedimentary facies is still at a low level, lacking fine-grained sand layer group sedimentary microfacies description. The understanding of sand body distribution is inadequate, seriously restricting the deep exploration process of the composite hydrocarbon reservoir. Based on these shortcomings, the authors studied the source and sedimentary facies characteristics of the Huagang Formation source–sink system in the central structural belt of the Y-area using the latest well–seismic data. This contribution aims to significantly improve the understanding of regional and micro-regional source–sink system patterns over the years, providing a detailed basis for exploration deployment.

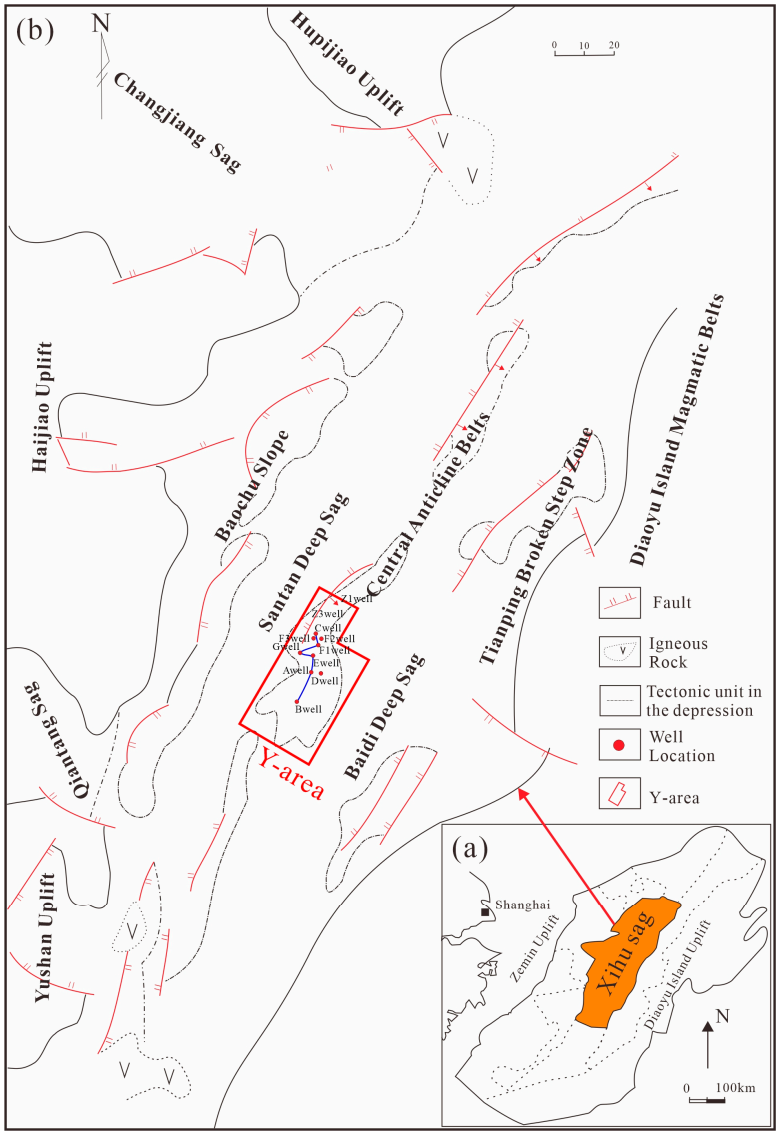


Figure 1. Tectonic location map of studied Y-area in the Xihu Sag (modified from the literature [11]). (**a**)The East China Sea Shelf Basin and Xihu Sag. (**b**) The Y-area at Xihu Sag.

2. Geological Background

The study area belongs to the northeast of the East China Sea Shelf Basin, extending towards the northeast and covering an area of approximately 5.2×10^4 km^2 [16]. It borders Hupijiao Uplift to the north, Haijiao Uplift to the west, Yushandong Low Uplift to the southwest, and the Diaoyu Island Upfold Belt [17] to the east. The parent rock type of northern Hupijiao Uplift is Proterozoic metamorphic quartzite, while those in the western Haijiao Uplift and eastern Yushandong Low Uplift are acidic to medium-acidic magmatic rocks from the Upper Cretaceous and Jurassic periods, respectively. The Diaoyu Island Upfold Belt to the east consists of medium-acidic magmatic rocks [18] from the Late Paleozoic to Mesozoic eras. The tectonic unit of the Xihu Sag exhibits characteristics [19] of a band in the east–west direction with divided north–south blocks. From west to east, five tectonic units were recognized: the Baochu Slope Zone, Santan Deep Depression, Central Anticlinal Zone, Baidi Deep Depression, and Tianping Fault-step Zone. The studied Y-area lies within a central northern part of the central anticlinal zone (Figure 1).

The East China Sea Shelf Basin has experienced five major tectonic movements throughout its geological history. Among these, the Yuquan movement at 35 Ma and the Longjing

movement at 5.2 Ma resulted in two significant regional unconformities, referred to as the T30 structural layer and T20 structural layer (Figure 2). These interfaces, along with the Tg surface of the Keelung movement (65 Ma), divide the tectonic evolution of the Xihu Sag into three stages: a rift period (Keelung–Yuquan, 65 Ma–35 Ma), depression period (Yuquan–Longjing, 35 Ma–5.2 Ma), and regional subsidence period (Longjing–present, 5.2 Ma–present) [20].

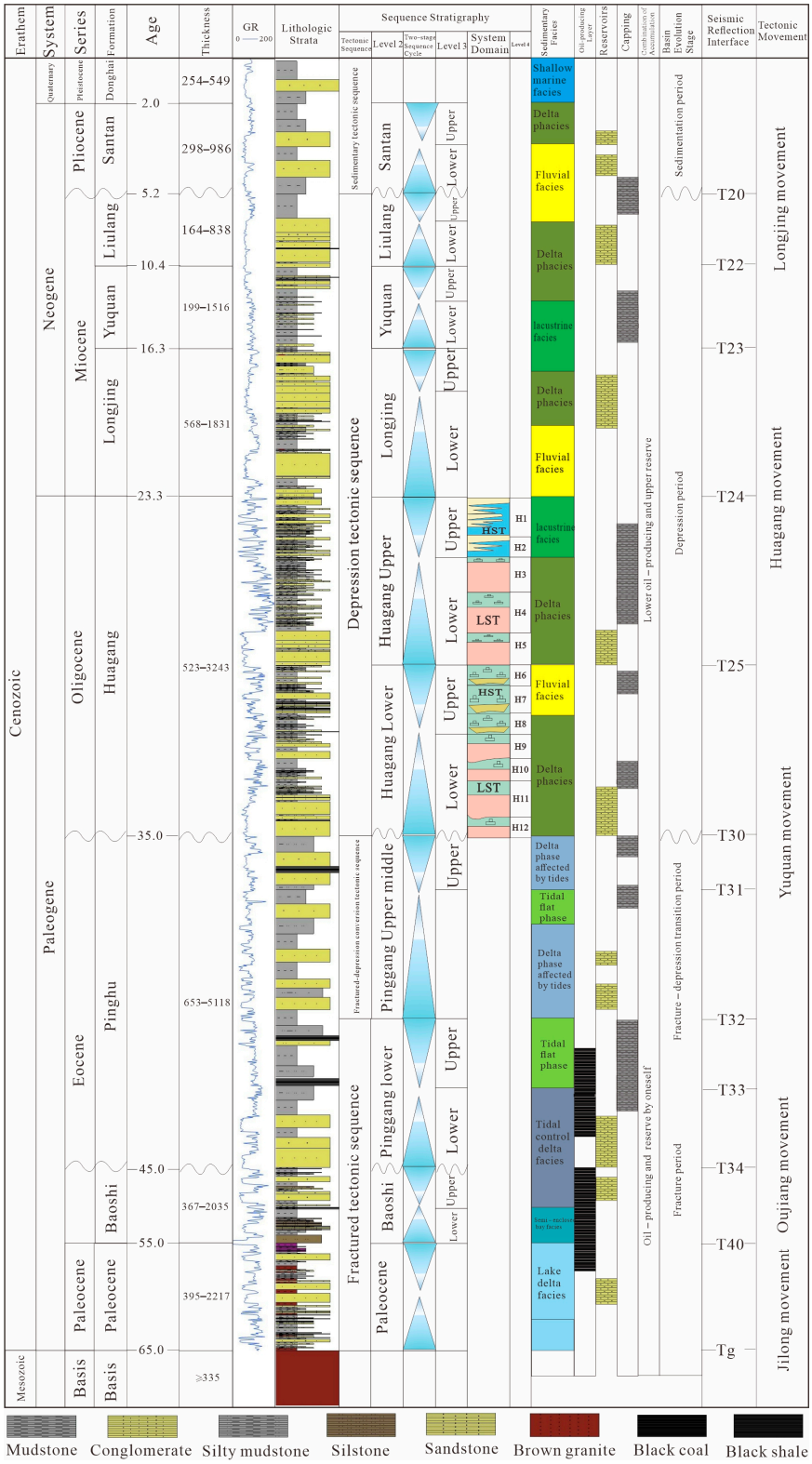


Figure 2. Comprehensive column chart of strata in the Xihu Sag.

After the Yuquan Movement, the Xihu Sag entered a period of depression, during which thick continental fluvio-delta-lacustrine sediments were deposited and filled, forming the present Huagang Formation [21]. The sedimentary period of the Huagang Formation in the Y-area was characterized by a warm and wet climate with shallow water bodies.

The Huagang Formation in the Y-area can be divided into two segments: the upper flower segment (H1–H3) and the lower flower segment (H4 and below). The H3–H7 portion is primarily composed of thick layers of fine sandstone, locally developed medium sandstone with some gravel, as well as a small amount of siltstone and mudstone. The H1–H2 segment consists mainly of mudstone and silty mudstone, occasionally interspersed with thin layers of siltstone and fine sandstone. The color variations in mudstone reflect frequent shifts between oxidizing and reducing environments.

3. Materials and Methods

This study combines the latest drilling results and analytical test data from the Y-area of the West Lake Depression over the past three years of research. The identification of microfacies is achieved through the analysis of seismic reflection characteristics, including amplitude, intensity, and continuity, in conjunction with logging data. Among the five new wells, D, F1, F3, and G provide more complete logging and analysis test data than the old wells, providing a solid data foundation for this study (Table 1). The elemental logging data of these four wells were analyzed to determine the ancient sedimentary environment of the Y-area. The statistical analysis of the 24 core samples and 116 cutting samples from the four wells determined the regional sediment source direction. At the same time, the 21 m core samples and 107 cast thin sections from nine wells in the area were observed and identified, clarifying the sedimentary microfacies developed in the Y-area. All tests were conducted at the Shanghai Experimental Center of the China National Offshore Oil Corporation. In this study, the sismic analysis software is DSG(10ep4.05), the formation and logging software is Resform Geooffice V3.5.

Table 1. List of analysis and laboratory items of the E, F1, F3, and G wells.

Well	Drilling Time	Granularity	Heavy Minerals	Elemental Logging	Cast Thin Sections	Core Samples	Cuttings Samples
E	17 July 2022–25 September 2022	62	19	/	54	24	41
F1	10 December 2022–18 December 2022	34	24	361	12	/	/
F3	22 January 2023–30 January 2023	40	41	261	19	/	24
G	8 February 2023–24 February 2023	26	14	197	22	/	51

4. Results

4.1. Sedimentary Facies

According to the well logging data, multiple wells in the H3–H7 segment of the Huagang Formation consist of thick sandstone with thin mudstone, and the sand/land ratio exceeds 40%, particularly the H3b2 thick sandstone with excellent lateral continuity, which is extensively developed in the area. The lithology is characterized by gray medium-fine sandstone, partially containing gravel aligned according to main axes within certain intervals. The sedimentary structures are predominantly characterized by massive bedding, tabular cross-bedding, parallel lamination, and wavy lamination. Scoured surfaces are commonly observed at the base of the riverbed. The C-M map (a graphical representation constructed using the C and M values derived from each sample, the C value represents

the particle size corresponding to 1% of the cumulative particle content in the particle size distribution curve, while the M value indicates the particle size corresponding to 50% of the cumulative curve, namely, the median particle size) lacks rolling components, while suspension population and jumping population are relatively well-developed, and the grain size probability diagram shows a typical two-stage pattern, which is judged to consist of channel deposition [22]. Multiple wells in the H1–H2 section of the Huagang Formation mainly comprise thin interlayers of variegated mudstone and silty sand rock. Comprehensive analysis suggests that braided river delta front sediments dominate the H3–H7 portion of the Huagang Formation (Figure 3), identifying four microfacies (Figure 4): an underwater distributary channel, estuary bar, sheet sand, and underwater distributary bay. During the depositional period of H1–H2, formation layers transformed into a meandering river sedimentary environment characterized by riverbed subfacies and river overflow subfacies.

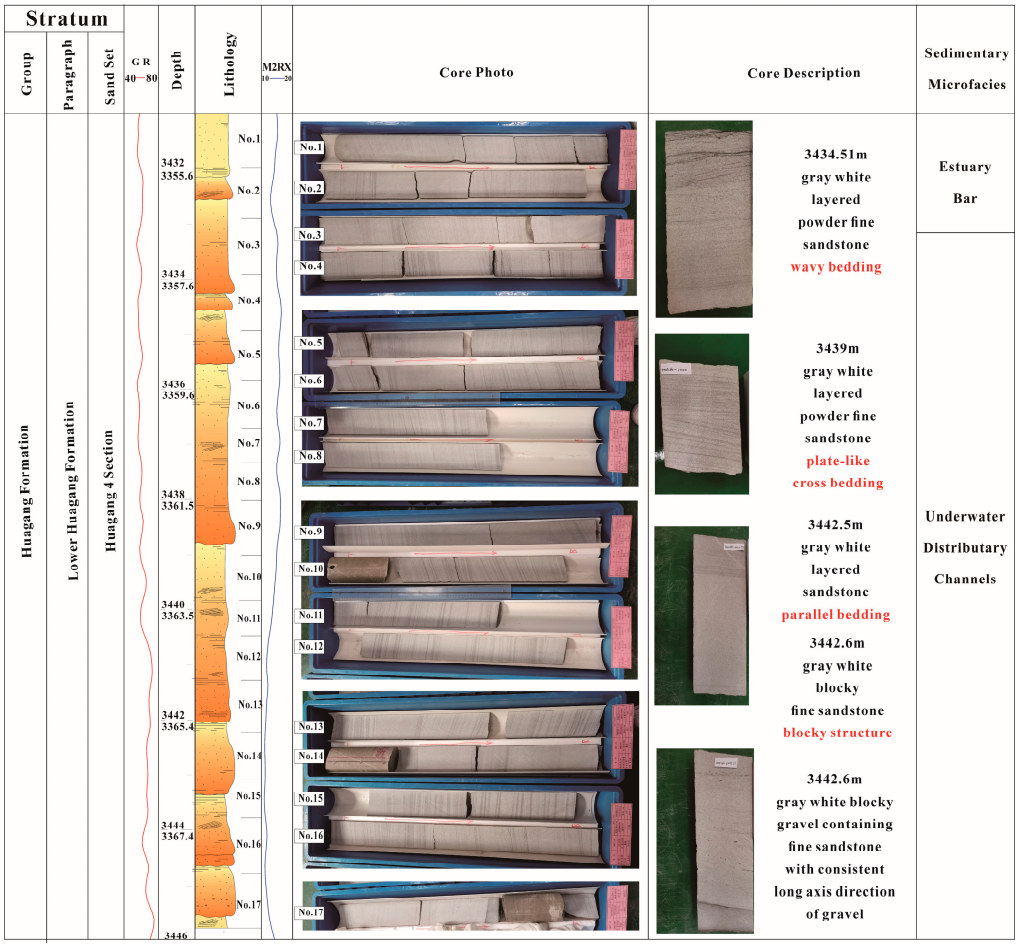


Figure 3. Core description of Section H4 of Well E.

4.1.1. Braided River Delta Front Subfacies (Figure 5a)

Microfacies of Subaqueous Distributary Channel

The lithology primarily comprises thick light gray fine sandstone interbedded with thin siltstone and mudstone. The GR curve exhibits a box-type and serrated bell shape, reflecting variations in water body energy (Figure 4). Lateral migration frequently occurs within the channel. The typical bedding structures observed in subaqueous distributary channels, including basal scour structures, massive bedding, parallel lamination, and tabular and wedge cross-bedding, can be identified through drilling operations. Seismic characteristics often display pronounced amplitude lenticular reflections.

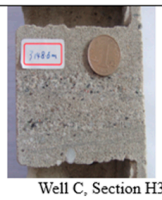
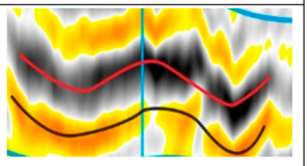
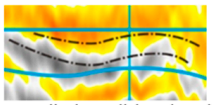
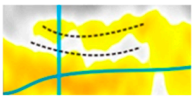
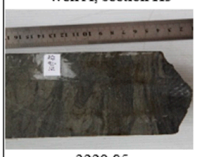
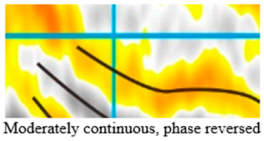
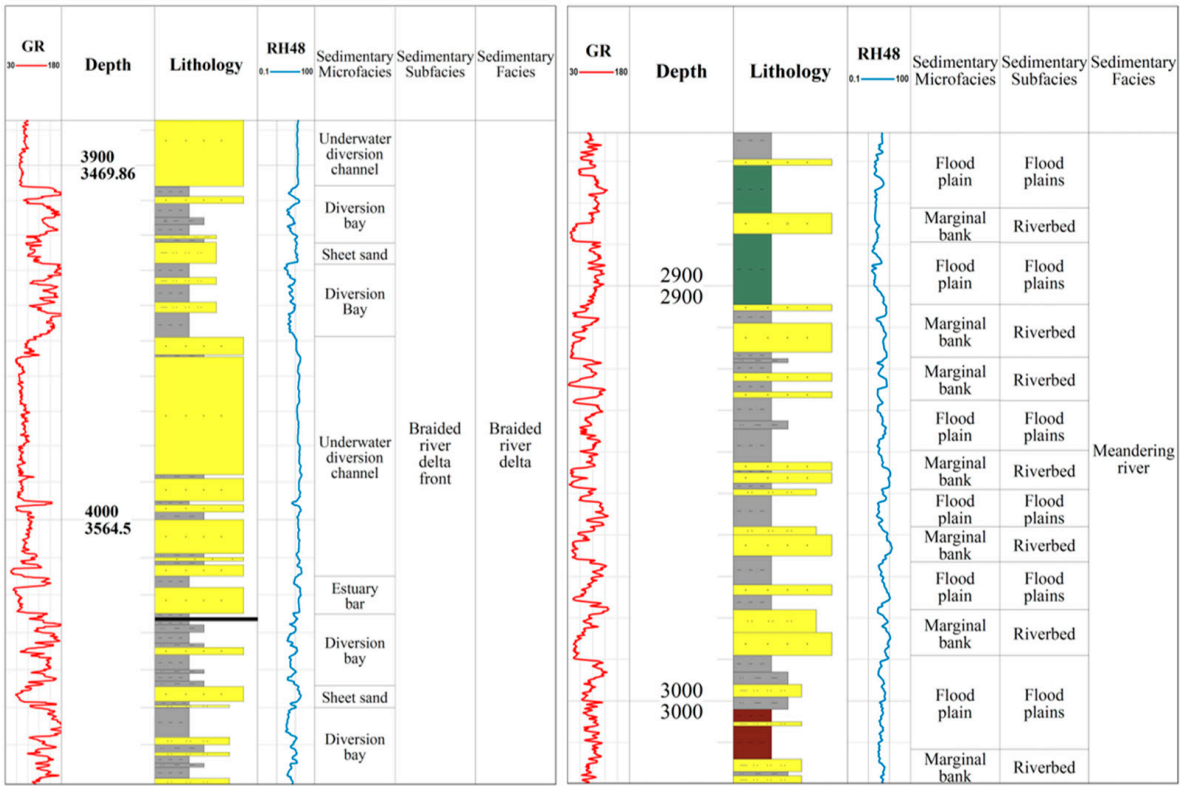
Sedimentary microfacies	Lithology and thickness	Bedding types and rhythmic characteristics	Drilling core	Logging phase		Seismic facies
Underwater fractions Stream channel	Gravelly sandstone, medium fine sandstone, mudstone and fine sandstone and sandstone combination 10 – 60m	Block structure, parallel bedding, plate and trough cross-bedding Positive rhythm	 Well C, Section H3 3148.6 m	GR curves are box, micro-toothed box and bell		 Strong amplitude lenticular reflection Parallel – subparallel seismic phases
Estuarine bar	Sorted, rounded good medium and fine sandstone 8 – 30m	Parallel bedding, plate bedding, trough cross-bedding Anti-rhythm	No corresponding drilling core	GR curve is funnel – shaped The amplitude is medium-high		 Medium amplitude parallel – subparallel seismic phase
Sheet sand	Light gray silty sand rock predominates 1 – 6m	Fine sandstone, silty sandstone, argillaceous siltstone Counter rhythm	No corresponding drilling core	The GR curve is zigzag Amplitude low - medium		 Weak amplitude parallel – subparallel seismic phase
Subaqueous shunt bay	Gray, dark gray mudstone, argillaceous siltstone and sand mud thin interbed 0 – 2m	Wavy bedding, horizontal bedding Positive rhythm	Well A, section H5  3229.85 m	The GR curve is low toothed		 Moderately continuous, phase reversed

Figure 4. Characteristics of sedimentary microfacies, petrofacies, logging facies, and seismic facies of the Huagang Formation in the Y-area.



(a)The section H5 of well F3 (b)The section H1 of well G

Figure 5. Electrical characteristics of rocks in the Huagang Formation, Y-area. (**a**) Electrical characteristics of delta front rock in section H5 of well F3. (**b**) Electrical characteristics of meandering river rock in H1 section of well G.

Estuarine Bar Microfacies

The lithology primarily consists of light gray medium-fine sandstone. The GR curve exhibits a funnel-shaped pattern with a high degree of dentition and medium-high amplitude, often displaying seismic reflection characteristics that are parallel–subparallel and of medium amplitude.

Sheet Sand Microfacies

The lithology comprises light gray silty sand rock characterized by a fine grain size, while the GR curve predominantly exhibits a funnel-shaped pattern with low to medium amplitude.

Underwater Diverging Bay Microfacies

The lithology primarily comprises gray mudstone and argillous siltstone, interspersed with thin layers of sand and mud. The GR curve exhibits a tooth-shaped pattern with low width and a continuous finger-type response, indicating multiple horizontal lines that signify repeated variations in low-energy water flow. Drilling core analysis enables the identification of undulating bedding and horizontal stratification.

4.1.2. Meandering River Subfacies (Figure 5b)

The deposition of H1 and H2 in the studied Y-area occurred during a period of rapid base-level decline, with meandering river sediments dominating the floodplain. The sand body exhibits a GR curve characterized by low bell and finger shapes, while drilling cores reveal interlayers of gray mudstone and fine sandstone with traces of bioturbation. Seismic data show parallel and subparallel reflections of medium to weak amplitude.

The mudstone of the H2 section of the Huagang Formation is green and gray-green as a whole, and the sandstone thickness is 20–40 m. However, the color of the mudstone in the H1 section gradually changed to mixed colors, the thickness of a single set of sandstone decreased significantly, and the thin interbedding of vertical and upper sandstone and mud appeared frequently.

4.2. Provenance

4.2.1. Petrological Characteristics

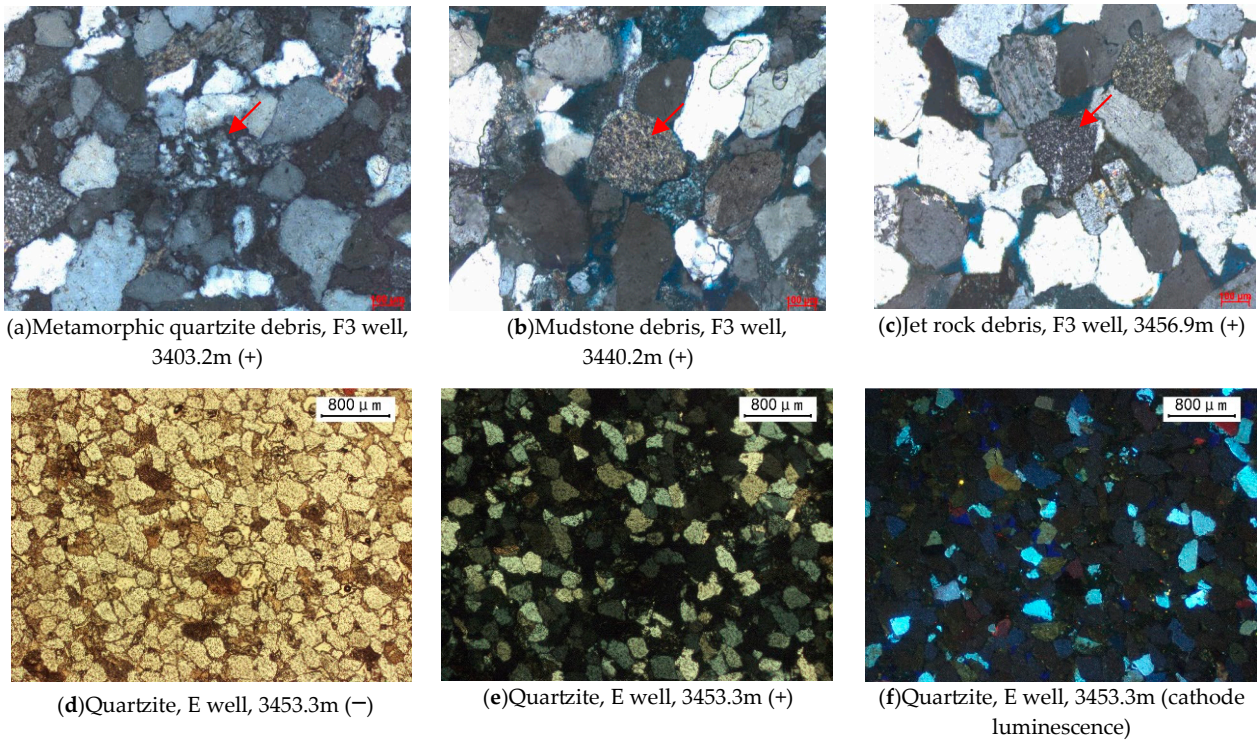
Gravel Composition and Cuttings Type

The parent rock type in the provenance area can generally be determined by analyzing the statistical terrigenous clastic assemblage in the basin [23]. Specifically, the characteristics of gravel in the conglomerate serve as important indicators for analyzing and determining the provenance area. Based on data from drilled core debris analysis, it is observed that mudstone and metamorphic quartzite are predominant constituents of gravel in the Y-area studied herein. Additionally, metamorphic quartzite and mudstone debris dominate, followed by magmatic rock debris. These findings suggest that metamorphic rock is likely to be the prevailing parent rock type in this area.

Characteristics of Quartz Cathode Luminescence

As one of the primary constituents of rocks, the luminescence of quartz varies depending on its source material. The observed color in the thin section of cathode-luminescent rock can be utilized to determine its origin [24]. Quartz derived from metamorphic rock typically emits brown light, while quartz originating from magmatic rock emits blue and purple light. Autogenetic-enlargement quartz generally does not exhibit any luminescence [15]. Through thin section observation, it is evident that most of the quartz in the Y-area is authigenic and non-luminescent. Some quartz displays brown luminescence, indi-

cating a predominantly metamorphic parent rock with some contribution from magmatic parent rocks (Figure 6).



(a)Metamorphic quartzite debris, F3 well, 3403.2m (+)

(**b**)Mudstone debris, F3 well, 3440.2m (+)

(**c**)Jet rock debris, F3 well, 3456.9m (+)

(**d**)Quartzite, E well, 3453.3m (−)

(**e**)Quartzite, E well, 3453.3m (+)

(**f**)Quartzite, E well, 3453.3m (cathode luminescence)

Figure 6. Thin sections characteristics of the Huagang Formation in the Y-area.

4.2.2. Heavy Mineral Characteristics

Heavy Mineral Combination Types

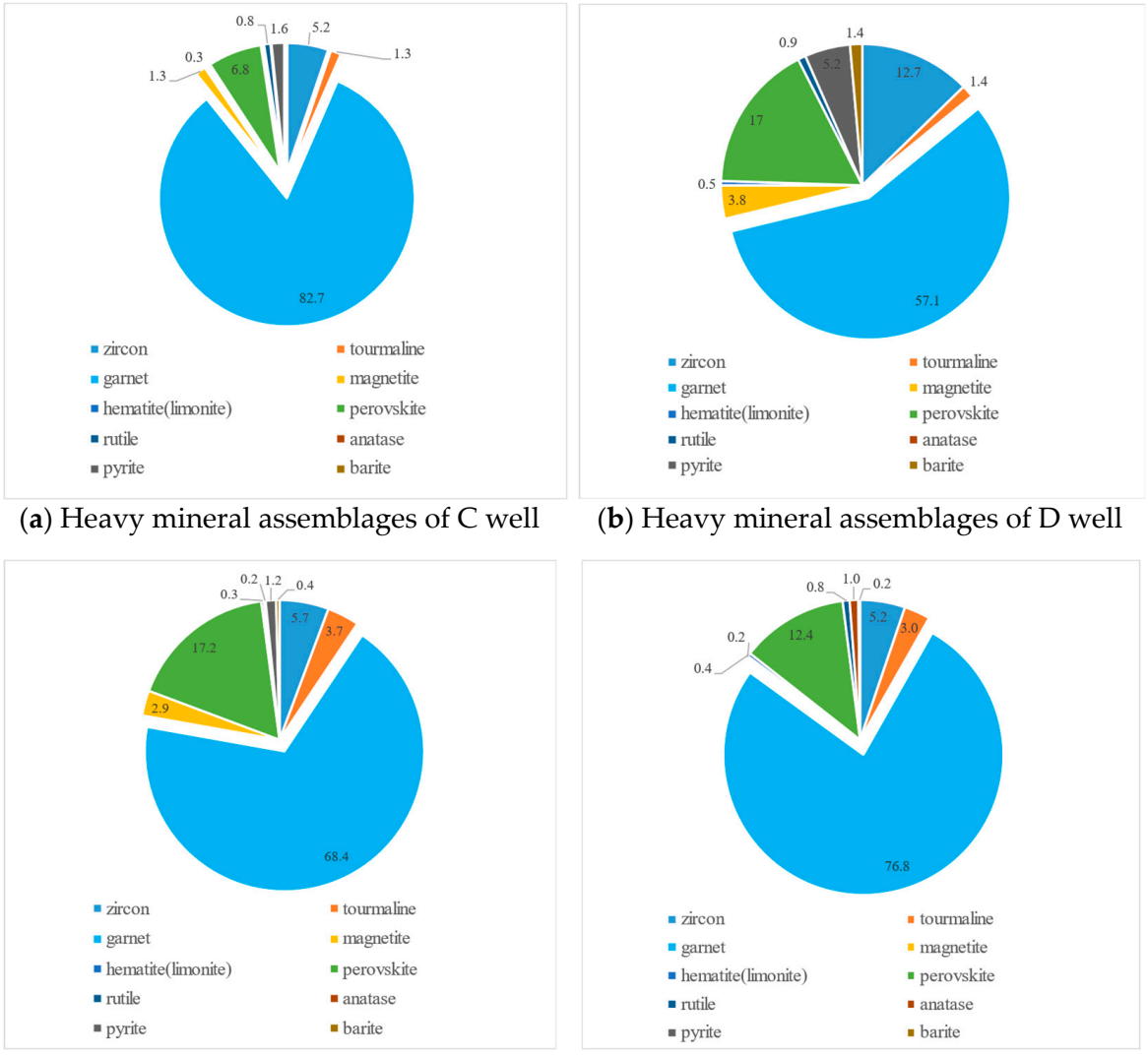
Due to variations in mineral components, different types of parent rocks yield distinct combinations of heavy minerals after weathering. For example, granite and granodiorite parent rock areas primarily produce zircon, sphene, apatite, and biotite. Garnet, kyanite, staurolite, and sillimanite are commonly found in metamorphic parent rock areas. However, sedimentary parent rock areas lack these characteristic heavy minerals [15]. In the Y-area, the heavy mineral assemblage mainly includes zircon, tourmaline, garnet, erythrolitmin, rutile, and pyrite, among others, with stable heavy minerals such as zircon, tourmaline, garnet, magnetite, titanite, rutile, etc., while unstable heavy minerals include pyrite, barite, and chlorite (Figure 7).

The predominant group of heavy minerals In the Y-area is garnet. Additionally, the rock in the wells contain magmatic-series heavy minerals like leucoxene, zircon, and tourmaline (Figure 7). Garnet content accounts for over 50% in each well and exhibits a gradual decline from north to south. Compared to the Q area near the western reef bulge within the central anticlinal belt region, where the content of the zircon–tourmaline–ilmenite series exceeds 60% in the Huagang Formation, with pyrite exceeding 10%, the Y-area has a significantly lower content of this series but an increased content of garnet, indicating that most of its provenance likely originates from the northwest Hupijiao Uplift, which is composed of metamorphic rocks. Furthermore, the presence of certain amounts of zircon, rutile, tourmaline, and ilmenites suggests a contribution from medium-acidic magmatic rocks.

ZTR Index

In practical applications, the stability of various heavy minerals exhibits significant variations. Generally speaking, zircon, tourmaline, and rutile are considered the most

stable minerals. The determination of parent rock transport distance can be achieved by calculating the proportion of these three minerals in relation to other heavy minerals, which is commonly referred to as the ZTR index. Typically, as we move away from the source area, there is an increased abundance of these three heavy minerals and consequently a higher value for the ZTR index. Overall, within our studied Y-area, there is a gradual increase in the ZTR index from north to south and from west to east. Based on our comprehensive analysis, incorporating regional ZTR index data along with paleo-geomorphology and heavy mineral association (Figures 7 and 8), it can be concluded that the Y-area has mixed sources characterized by a dominant northeast-oriented long-axis source supplemented by a west-oriented short-axis source.



(**a**) Heavy mineral assemblages of C well (**b**) Heavy mineral assemblages of D well

(**c**) Heavy mineral assemblages of E well (**d**) Heavy mineral assemblages of F3 well

Figure 7. Analysis of heavy minerals in the Y-area.

4.2.3. Distribution Characteristics of Sedimentary Facies

Distribution Characteristics of Sedimentary Facies Profile

The sedimentary characteristics of the Huagang Formation are illustrated in Figure 8, along with the well profile connecting wells B–A–E–G–F1–C (refer to Figure 1 for survey line location). In the lower part of the Huagang Formation, a dominant continental shallow-water lake-delta environment is observed. In the context of the deposition of the lower Huagang section, the Y-area represents the forefront of braided river delta sedimentation.

H4–H7 sandstone formations exhibit thick, continuous, and widespread distribution. Multiple underwater distributary channels intersect and overlap each other, with grain size gradually decreasing and eventually forming gray mudstone deposits. Coarse debris is relatively scarce at the base of the upper part of the Huagang Formation. Thick-layered sandstones display toothed box logging facies, while thin-layered sandstones show multi-fingered patterns, indicating predominantly braided river delta-fluvial facies deposits. Between well C and well F1 during the H3 segment deposition period, it is believed that a transition occurred from braided river delta plain subfacies to braided river delta front subfacies. A braided river delta front developed near and southward from well F1, continuously unloading sediment towards well B, resulting in thinner sandstone layers mainly composed of sand–mudstone interlayers. Vertically, the facies transition from the braided river delta of the H3 segment to the meandering river deposits of the H1-H2 segments is observed.

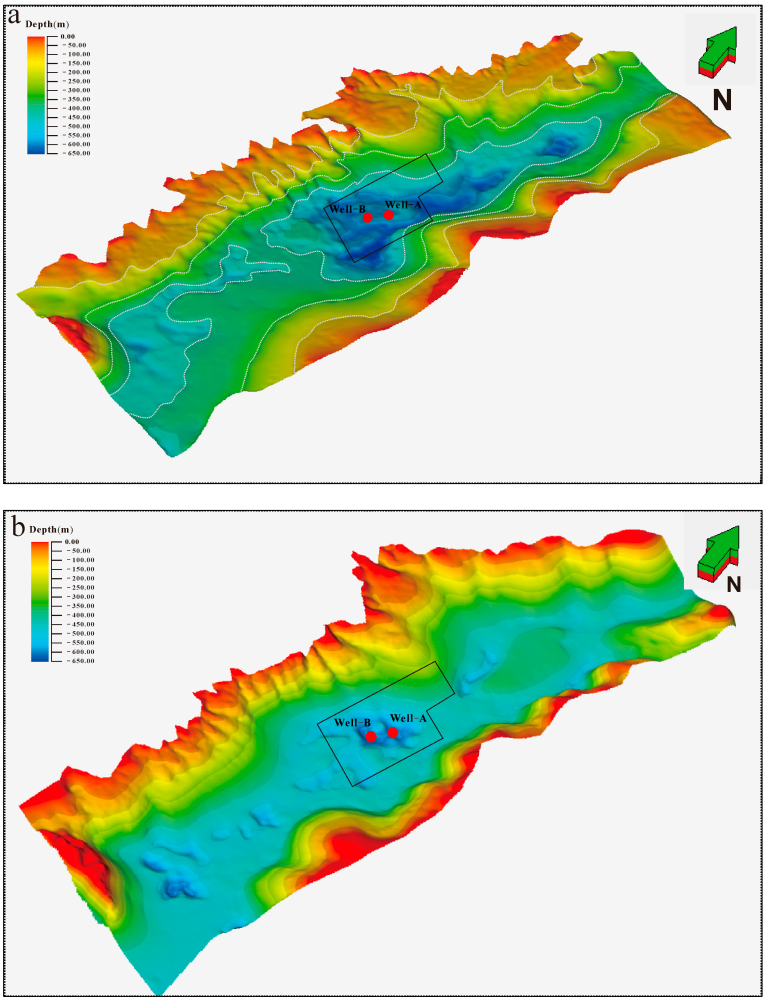


Figure 8. Paleo-geomorphological map of the Huagang Formation in the Y-area. (**a**) Paleo-geomorphological map of the upper Huagang Formation. (**b**) Paleo-geomorphological map of the lower Huagang Formation.

Characteristics of Planar Distribution of Sedimentary Facies

Based on the working experience in this area, the RMS amplitude attribute effectively distinguishes between sand and mudstone, accurately predicting sand bodies that align with actual drilling results. Extracting multiple sets of RMS amplitude attributes from the Huagang Formation elucidates the planar distribution characteristics of sedimentary facies (Figure 9).

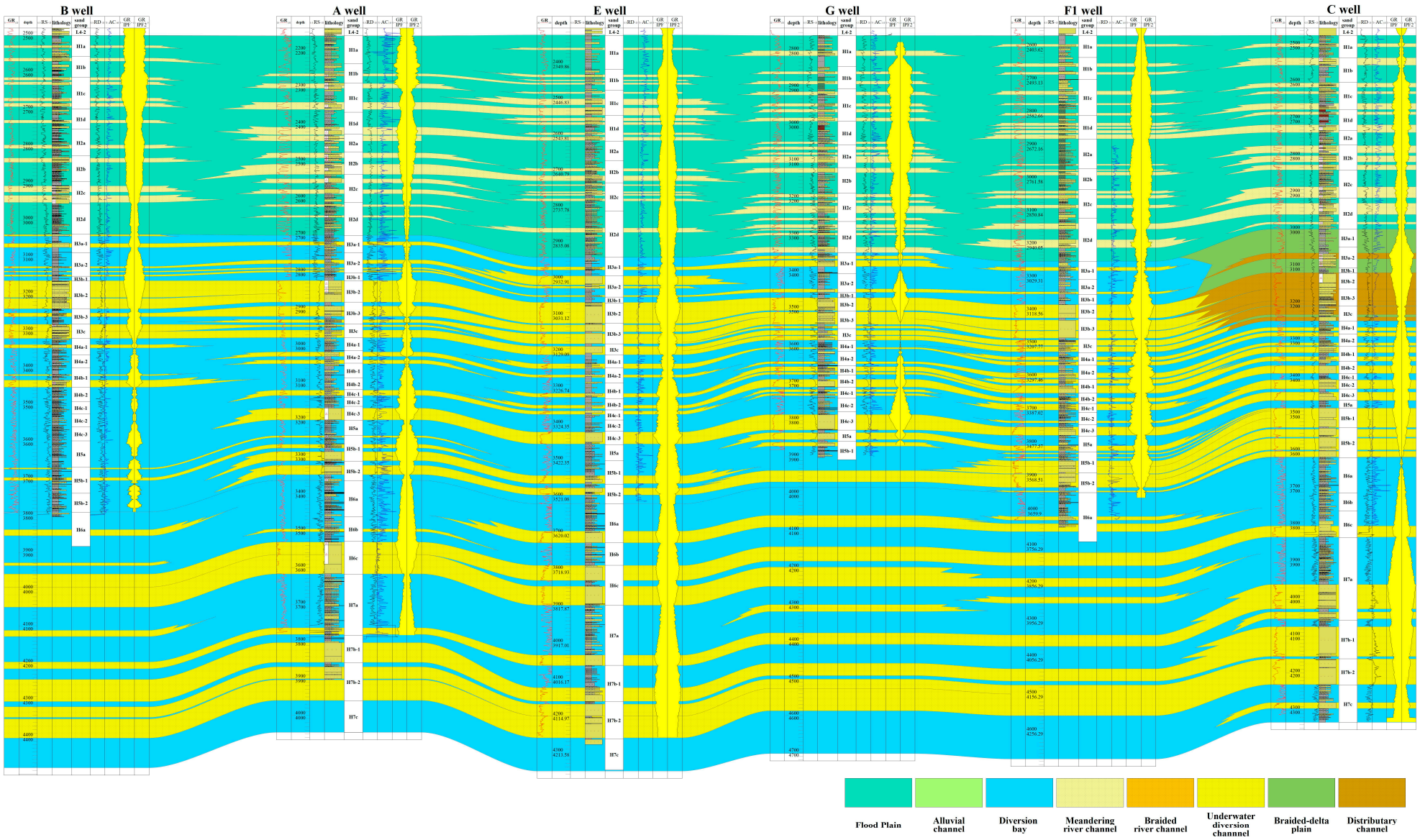
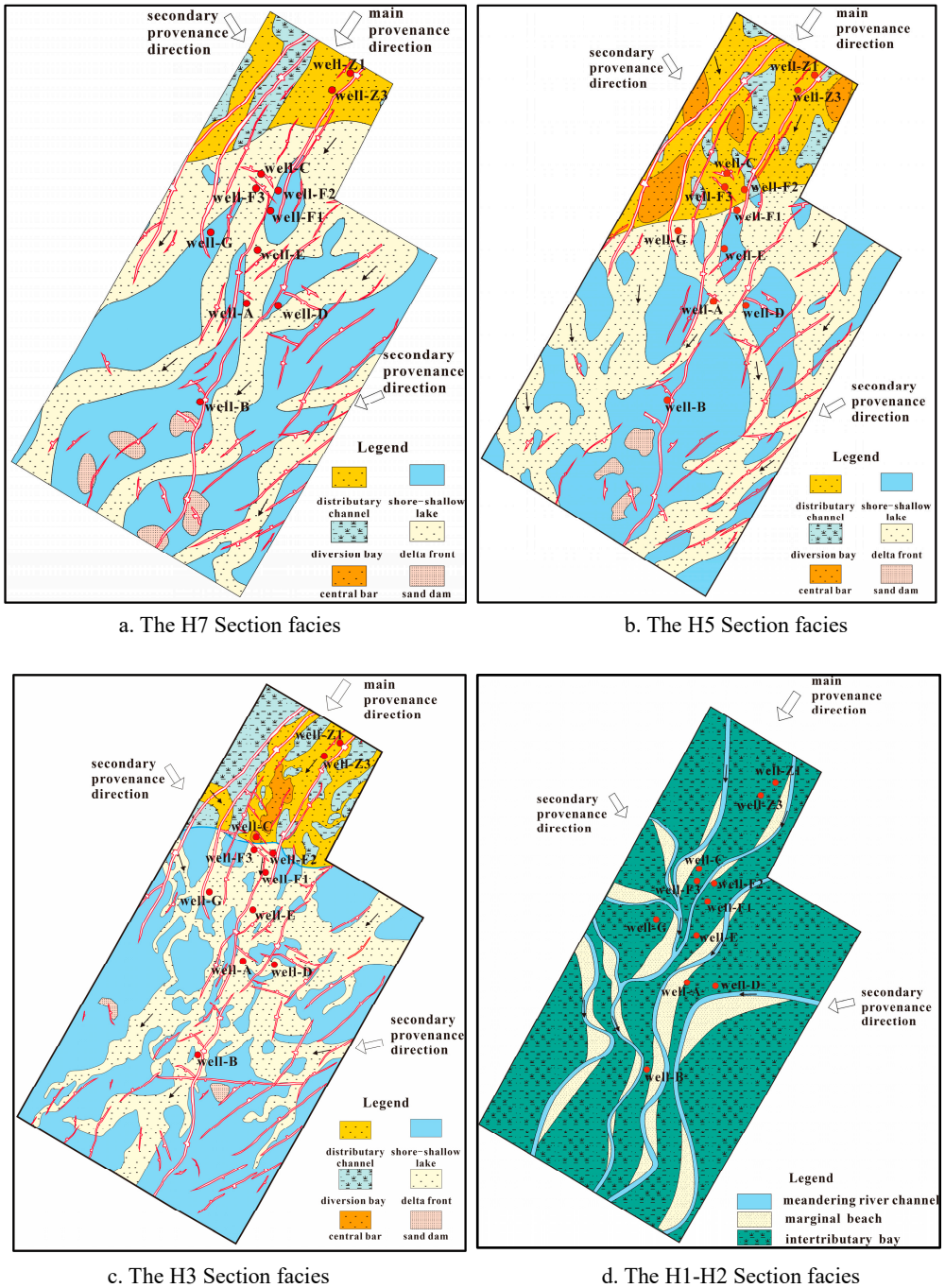


Figure 9. Profile of sedimentary facies of the Huagang Formation in the Y-area (see Figure 1 for the position of the profile).

During the deposition period of segment H7–H4, there was a continuous deepening of the water body, resulting in longitudinally developed thick box sands that formed uninterrupted sheets, primarily deposited within underwater distributary channels and interdistributary bays. Estuary bar sedimentation also exhibited significant development. In the deposition period of section H3, as the water body became shallower and the lake plane shrank towards the vicinity of well C, plain sedimentation occurred in well C and northern areas characterized by coarser sandstone grain size and higher sand/area ratio. The transition from braided river delta plain to delta front-lake deposition took place progressively from north to south across the entire area, where deltaic sand bodies thinned out and reached their peak thicknesses from east to south (Figure 10).



a. The H7 Section facies

b. The H5 Section facies

c. The H3 Section facies

d. The H1-H2 Section facies

Figure 10. Sedimentary facies plan of the Y-area.

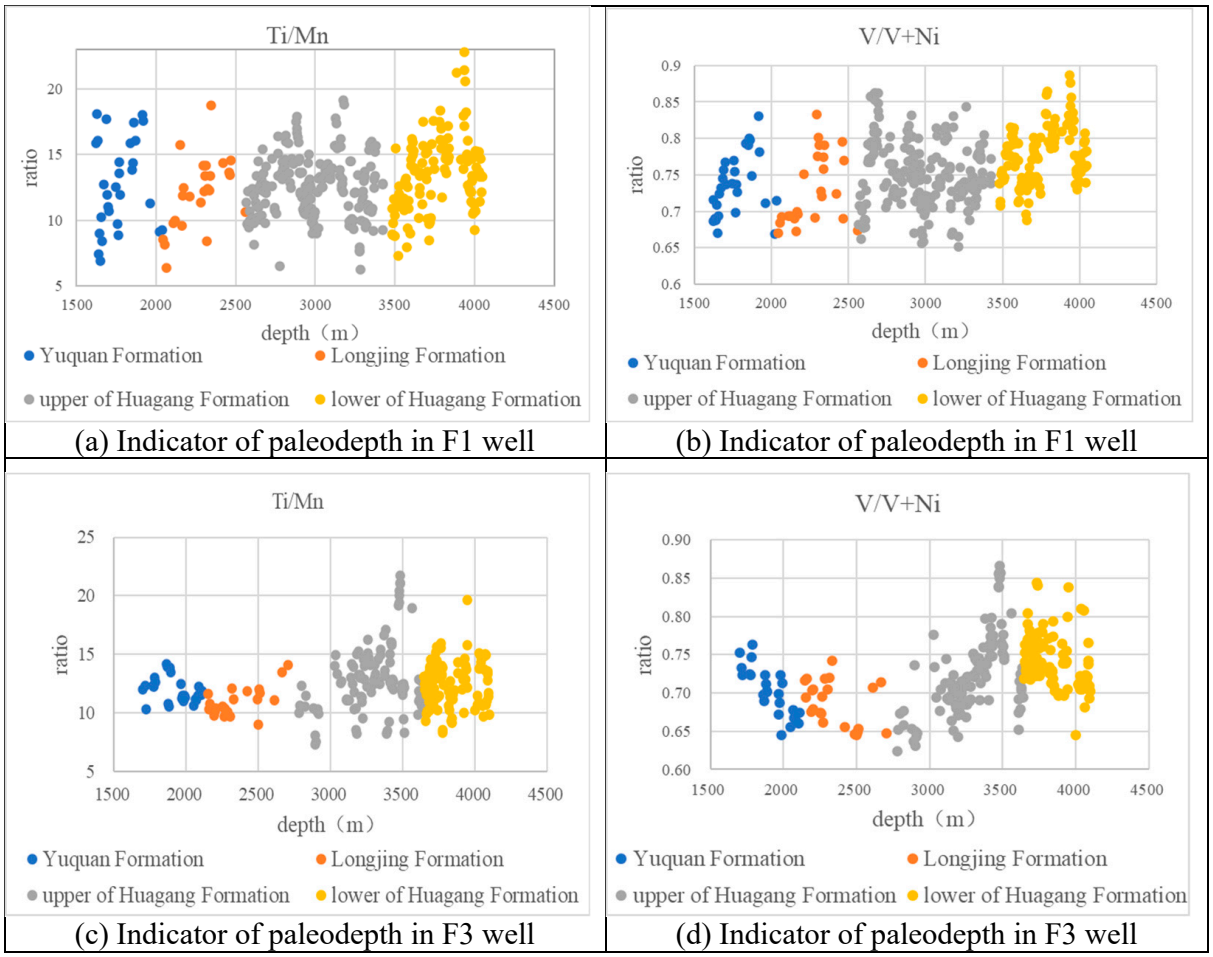
5. Discussion

5.1. Paleo-Environment

According to the regional paleo-water depth reconstruction, the lower Huagang Formation exhibits an average water depth of 23 m, whereas the upper Huagang Formation demonstrates an average water depth of 12 m. Both formations represent terrestrial shallow sedimentary environments [25]. This perspective is substantiated by analyzing geochemical indices obtained from recent drilling activities in the Y-area.

The geochemical element indices of wells F1, F3, and G suggest that the Y-area represents a nearshore shallow-water anaerobic reduction environment.

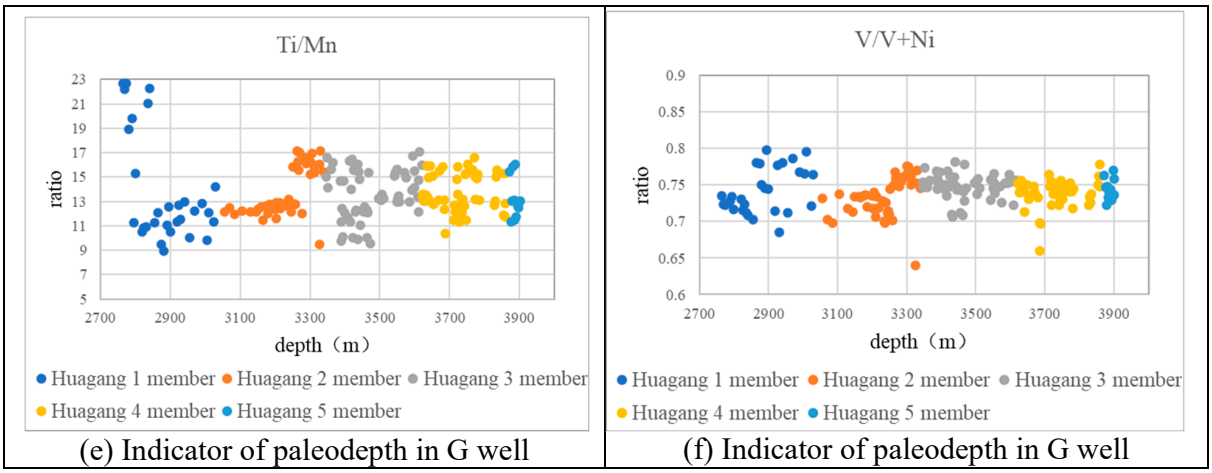
Generally, Mn exhibits greater stability than Ti during sediment transport, and the Ti/Mn ratio can serve as an indicator of the sedimentary environment (Figure 11). In deep-water settings, the Ti/Mn ratio is 3.3 lower compared to general conditions. However, in nearshore shallow-water environments, the Ti/Mn ratio generally exceeds 10 [25]. The V/(V+Ni) ratio can be utilized to characterize paleo-redox conditions. In anaerobic reduction environments, V/(V+Ni) surpasses 0.6, while in oxygen-rich sedimentary environments, it typically falls below 0.46 [26].



(a) Indicator of paleodepth in F1 well (b) Indicator of paleodepth in F1 well

(c) Indicator of paleodepth in F3 well (d) Indicator of paleodepth in F3 well

Figure 11. *Cont.*



(e) Indicator of paleodepth in G well (f) Indicator of paleodepth in G well

Figure 11. Analysis diagram of paleo-environmental geochemical element index in Y-area.

5.2. Hydrocarbon Exploration

The West Lake Depression in the East China Sea Shelf Basin has been subject to oil and gas exploration for over 60 years, with the initial discovery of the Pinghu 1 well occurring 50 years ago. Over the past four decades, exploration and research have extended southwards from the west slope zone of the Xihu Sag to the saddle uplift structural zone of the Xihu Sag–Jilong Depression, resulting in significant findings, such as the Chunxiao 1 well and Chunxiao gas field. Currently, there is widespread attention on investigating the favorable lithologic reservoir facies belt of the Huagang Formation, along with its exploration direction, discoveries, and research [27].

This recognition of the need for exploration represents a significant advancement. Initially, the understanding was based on conventional theory, as the Xihu Sag is characterized by a fault basin that spreads almost north–south, with the east and west slope belts identified as primary and secondary sources of natural materials. However, further exploration revealed that sand–argillaceous interaction deposits formed in both the northern valley facies and southern alluvial plain facies, with an effective sedimentary sand body thickness reaching hundreds of meters. Surprisingly, despite being low in the middle of the basin, the sand body exhibited exceptional thickness.

At 43 Ma, a comprehensive collision occurred between the Pacific–Philippine Sea plate and the Eurasian plate, resulting in changes in convergence rate and direction. This collision initially caused southeastern movement of the Asian plate, leading to regional plate position adjustment and significant tectonic recombination in the East China Sea Shelf Basin. The Pacific plate was subducted from the NW to the Eurasian plate. At 25 Ma, counterclockwise rotation of the southern end of the Philippine Sea subduction zone [28] and collision between the northern end of Australian plate and the arc-continent resulted in tectonic–sedimentary response in eastern basins of China's mainland, including the Bohai Bay Basin and the East China Sea Shelf Basin, forming an important tectonic change interface [29]. At 24 Ma, collision between the Australian plate and the northern island arc of New Guyana produced a northward movement of the Philippine Sea plate, which became embedded between the Eurasian plate and Pacific plate, forming the Huagang movement (Figure 1).

The northward movement of the Philippine Sea plate has caused the Luzon Island Arc to collide with the Eurasian plate in southern Taiwan, resulting in a northwestward displacement of Taiwan Island at a speed of 48 mm/a [30]. This tectonic activity has significantly influenced the Xihu Sag in the East China Sea Shelf Basin since the Middle Miocene. The left-lateral-extrusion Longjing movement is attributed to the northwest–

western motion of the Philippine Sea plate (Figure 1). The intense compression generated by this movement has led to tectonic inversion within the basin, with greater intensity observed in its northeast region and lesser intensity in central and southern parts. Strata denudation is prominent in northeastern areas but minimal in southwestern regions. Fission track technology was employed to calculate different drilling structure reversal periods, revealing substantial denudation ranging from 491 to 1786 m during Late Miocene times [31,32]. Therefore, these structural reversals and extensive denudation have rendered the Huagang Formation an important target for exploration.

Secondly, the investigation of topography, geomorphology, and sedimentary facies features in the Xihu Sag is highly robust. By examining regional paleo-water depth restoration, it has been determined that the average water depth of the lower Huagang section is 23 m, while the upper Huagang section exhibits an average water depth of 12 m; both indicate shallow terrestrial sedimentary environments. This perspective is corroborated by analyzing geochemical indices from new drilling conducted in the Y-area. Additionally, it has been demonstrated that Mn displays greater stability compared to Ti during sediment transport. The Ti/Mn ratio indicates a depositional environment. In the deep-water sedimentary environment of the far coast, the Ti/Mn ratio is 3.3 lower than that observed in general. In the nearshore shallow-water sedimentary environment, the Ti/Mn ratio tends to exceed 10 [25]. Furthermore, within paleo-redox environments characterized by vanadium–nickel ratios, V/(V+Ni) values exceeding 0.6 are indicative of anaerobic reduction conditions, whereas oxygen-rich sedimentary environments generally exhibit values below 0.46 [26]. Through analysis of geochemical element indexes obtained from wells F1, F3, and G, it was observed that the Huagang Formation can be divided into two intervals: an upper interval encompassing H1–H3 and a lower interval comprising H4 and below. Notably, within these intervals (H3–H7), thick layers of fine sandstone prevail, with localized occurrences of medium sandstone containing some gravel as well as minor amounts of siltstone and mudstone present. On the other hand, sections H1–H2 predominantly consist of mudstone and silty mudstone intercalated with thin layers of siltstone and fine sandstone, exhibiting frequent variations in oxidation–reduction colors within the mudstones' composition, and consequently establishing definitive characteristics representative of nearshore shallow-water anaerobic reduction environments in the Y-area (Figure 10).

The compression in the T30 period caused the Xihu Sag to move from depression to uplift, as well as a reversal of the anticlinal structure from the depositional center to the central long wall structure of the West Lake Depression, which is crucial for identifying lithologic complex hydrocarbon reservoirs. Additionally, the sandstone reservoir system in the Y-area is determined by both source–sink systems and sedimentary facies. This paper presents recent research findings that have garnered significant attention and deepened our understanding at both macro- and micro-levels.

6. Conclusions

Most of the quartz in the Y-area does not emit light and is self-generated. Some of the quartz glows brown and a small part glow blue, indicating that the parent rock mainly comes from metamorphic rock, with a magmatic parent rock supplement. Combined with the characteristics of heavy minerals in the study area, the Huagang Formation in the Y-area of Xihu Sag is predominantly derived from the long-axis provenance of Hupijiao Uplift in the northeast, with supplementary contributions from the short-axis provenance of the West Sea Reef Bulge.

Through the observation of the drilling core in the area and the analysis of the characteristics of the logging curve, the Huagang Formation within the studied Y-area mainly

comprises onshore fluvial lacustrine facies deposits, which can be categorized into four high-precision sequences characterized by a meandering river sedimentary system in segments H1–H2 and braided river delta sedimentary system in segments H3–H7.

Geochemical analysis conducted on wells F1, F3, and G indicates that the Ti/Mn ratio mostly exceeds 10 and the V/(V + Ni) ratio surpasses 0.6, suggesting a predominantly anaerobic reduction environment near the coast during that specific period.

During the deposition period of H3–H7, the predominant sediment in the Y-area was the braided river delta front. The development of braided river delta plain subfacies only occurred near well C in the northern part of the Y-area. There was a transition in sedimentary facies from north to south, with a change from braided river delta plain subfacies to braided river delta front-lake facies. The thickness and peak of the delta sand body decreased progressively from east to south. During the H1–H2 deposition period, a meandering river sedimentary system dominated in the Y-area, primarily characterized by thick mottled mudstone interbedded with thin layers of fine sandstone.

Author Contributions: Conceptualization, X.M. and H.X.; methodology, X.M. and W.Y.; software, investigation, C.Y., S.Z.; data collection and analysis, Y.Y., R.S., and D.S.; writing—original draft preparation, X.M.; writing—review and editing, X.M., H.X., and W.Y.; literature investigation, Y.C. and G.Z. (Guoqing Zhang); technical support, G.Z. (Guangxue Zhang) and G.Z. (Guoqing Zhang). All authors have read and agreed to the published version of the manuscript.

Funding: This research was funded by projects of the National Natural Science Foundation of China (No. 49206061; No. 41106064); National Major Science and Technology Projects for Oil and Gas (No. 2011ZX05025-002-04); National Science and Technology Basic Resources Survey Project (No. 2017FY201407); Basic and Applied Research Foundation of Guangdong Province (No. 2022A1515110395); Hainan Province Natural Science Foundation Project (No. 423MS132); key project of the National Natural Science Foundation (No. 42130408); Consulting Project of the China Engineering Science and Technology Development Strategy Hainan Research Institute (No. 25HNZX-06); and Geological Investigation Programs of China Geological Survey (No. DD20230646).

Institutional Review Board Statement: Not applicable.

Informed Consent Statement: Not applicable.

Data Availability Statement: Data is contained within the article.

Acknowledgments: We would like to express our gratitude to the Exploration and Development Research Institute of the Shanghai Offshore Oil and Gas Branch of SINOPEC for their valuable contributions and provision of data.

Conflicts of Interest: Author Xiao Ma, Yi Yang, Ru Sun, Yue Chao, Chao Yang and Shudi Zhang were employed by the company Shanghai Offshore Oil and Gas Branch of SINOPEC. Wei Yan, Guoqing Zhang and Guangxue Zhang were employed by the company Guangzhou Marine Geological Survey. The remaining authors declare that the research was conducted in the absence of any commercial or financial relationships that could be construed as a potential conflict of interest.

Abbreviations

E3h3	the third section of Huagang Fotmation in Oligocene
E3h4	the fourth section of Huagang Fotmation in Oligocene
E3h5	the fifth section of Huagang Fotmation in Oligocene
T30	T30 structural layer
T20	T20 structural layer
H1	the first section of Huagang Formation (Upper Member of Huagang Formation)
H2	the second section of Huagang Formation (Upper Member of Huagang Formation)
H3	the third section of Huagang Formation (Upper Member of Huagang Formation)
H4	the fourth section of Huagang Formation (Lower Member of Huagang Formation)

H5	the fifth section of Huagang Formation (Lower Member of Huagang Formation)
H7	the seventh section of Huagang Formation (Lower Member of Huagang Formation)
H3b2	b2 single sand body of the third Huagang sand layer group
RMS	root-mean-square

References

1. Xu, F.; Xu, G.; Liu, Y.; Zhang, W.; Cui, H.; Wang, Y. Factors controlling the development of tight sandstone reservoirs in the Huagang Formation of the central inverted structural belt in Xihu Sag, East China Sea Basin. *Pet. Explor. Dev.* **2020**, *47*, 101–113. [CrossRef]
2. Hu, M.Y.; Li, S.Z.; Dai, L.M.; Suo, Y.; Guo, L.; Somerville, I.; Liu, Z.; Ma, F. Dynamic mechanism of tectonic inversion and implications for oil-gas accumulation in the Xihu Sag, East China Sea Shelf Basin: Insights from numerical modelling. *Geol. J.* **2018**, *53*, 225–239. [CrossRef]
3. Hao, L.; Wang, Q.; Guo, R.; Tuo, C.; Ma, D.; Mou, W.; Tian, B. Diagenetic fluids evolution of Oligocene Huagang Formation sandstone reservoir in the south of Xihu Sag, the East China Sea Shelf Basin: Constraints from petrology, mineralogy, and isotope geochemistry. *Acta Oceanol. Sin.* **2018**, *37*, 25–34. [CrossRef]
4. Wang, W.; Lin, C.; Zhang, X.; Dong, C.; Ren, L.; Lin, J. Effect of burial history on diagenetic and reservoir-forming process of the Oligocene sandstone in Xihu sag, East China Sea Basin. *Mar. Pet. Geol.* **2020**, *112*, 104034. [CrossRef]
5. Sun, X.L.; Lin, C.Y.; Zhang, X.G.; Lin, J.L.; Zhao, Z.X.; Huang, D.W.; Duan, D.P. Characteristics and distribution of clay minerals and their effects on reservoir quality: Huagang Formation in the Xihu Sag, East China Sea Basin. *Aust. J. Earth Sci.* **2019**, *66*, 1163–1174. [CrossRef]
6. Qian, W.D.; Sun, Q.L.; Stuart, J.J.; Yin, T.; Zhang, C.; Xu, G.; Hou, G.; Zhang, B. Diagenesis and controlling factors of Oligocene Huagang Formation tight sandstone reservoir in the south of Xihu Sag, the East China Sea Shelf Basin. *J. Pet. Sci. Eng.* **2022**, *215*, 110579. [CrossRef]
7. Zhou, X.; Xu, G.; Cui, H.; Zhang, W. Fracture development and hydrocarbon accumulation in tight sandstone reservoirs of the Paleogene Huagang Formation in the central reversal tectonic belt of the Xihu Sag, East China Sea. *Pet. Explor. Dev.* **2020**, *47*, 499–512. [CrossRef]
8. Yang, F.; Wang, M.; Zhuang, J. Kinematical processes of inversion structure and its contribution to hydrocarbon accumulation in Xihu Depression of East China Sea Basin. *Acta Pet. Sin.* **2010**, *31*, 596–601. [CrossRef]
9. Tao, S.Z.; Zou, C.N. Accumulation and distribution of natural gases in Xihu Sag, East China Sea Basin. *Pet. Explor. Dev.* **2005**, *32*, 103–110. [CrossRef]
10. Yang, W.; Yong, Q.; Liu, Y.; Liu, S.; Elsworth, D.; Zhang, R. Organic Geochemical and Petrographic Characteristics of the Coal Measure Source Rocks of Pinghu Formation in the Xihu Sag of the East China Sea Shelf Basin: Implications for Coal Measure Gas Potential. *Acta Geol. Sin. (Engl. Ed.)* **2020**, *94*, 364–375.
11. Shen, Y.L.; Qin, Y.; Cui, M.; Xie, G.; Guo, Y.; Qu, Z.; Yang, T.; Yang, L. Geochemical Characteristics and Sedimentary Control of Pinghu Formation (Eocene) Coal-bearing Source Rocks in Xihu Depression, East China Sea Basin. *Acta Geol. Sin. (Engl. Ed.)* **2021**, *95*, 91–104. [CrossRef]
12. He, J.; Wang, T.; Tang, Y.; Zhang, D.; Zhang, T.; Diao, H.; Liu, B.; Hu, Y. Geochemical characteristics and gas-washing accumulation mechanism of hydrocarbon from the Xihu Sag, East China Sea Basin. *Geoenergy Sci. Eng.* **2023**, *224*, 211639. [CrossRef]
13. Xu, H.; Hou, D.; Cao, B.; Chen, X.; Xu, T. Geochemical characteristics of high-maturity crude oils in the Xihu Depression, East China Sea Basin. *Geochem. J.* **2016**, *50*, 163–178. [CrossRef]
14. Cheng, Y.; Wu, Z.; Xu, B.; Zhang, J.; Chu, Y.; Dai, Y.; Xu, L.; Sun, W.; Ma, S. Structural characteristics and genetic mechanism of transfer zones in an extensional rift zone: An example from the Xihu Sag, East China Sea Basin. *Tectonophysics* **2023**, *856*, 229852. [CrossRef]
15. Lou, M.; Cai, H.; He, X.; Liu, Y.; Huang, X.; Zhang, X.; Liu, H. Application of seismic sedimentology in characterization of fluvial-deltaic reservoirs in Xihu sag, East China Sea shelf basin. *Pet. Explor. Dev.* **2023**, *50*, 138–151. [CrossRef]
16. Zhang, J.P.; Yu, Y.F.; Zhang, T.; Zhang, S.; Tang, X. A discussion on the exploration potential of deep basin gas in Xihu Sag, East China Sea. *China Offshore Oil Gas* **2023**, *24–29*, 35. (In Chinese with English abstract)
17. Chen, S. Main geological characteristics and gas exploration directions in East China Sea Basin. *China Offshore Oil Gas (Geol.)* **2003**, *17*, 6–13.
18. Liu, J.; Li, S.; Liao, K.; Cui, Y.; Shao, L.; Qiao, P.; Lu, Y.; Hou, Y.; Goh, T.L.; Yao, Y. New interpretation on the provenance changes of the upper Pinghu–lower Huagang Formation within Xihu Depression, East China Sea Shelf Basin. *Acta Oceanol. Sin.* **2023**, *42*, 89–100. [CrossRef]
19. Peng, W. Diaoyu Islands folded-uplift belt evolution characteristics and its importance on the hydrocarbon exploration in East China Sea basin. *Pet. Geol. Eng.* **2012**, *26*, 10–14.

20. Wang, W.J.; Li, G.; Yang, C.Q.; Yang, C. Characteristics of seismic sequence in the East China Sea shelf basin and their geological attributes. *Mar. Geol. Quat. Geol.* **2013**, *33*, 117–122, (In Chinese with English abstract). [CrossRef]
21. Cukur, D.; Horozal, S.; Kim, D.C.; Han, H.C. Seismic stratigraphy and structural analysis of the northern East China Sea Shelf Basin interpreted from multi-channel seismic refection data and cross-section restoration. *Mar. Petrol. Geol.* **2011**, *28*, 1003–1022. [CrossRef]
22. Jiang, Z.X. *Sedimentology*; Petroleum Industry Press: Beijing, China, 2003; pp. 1–424. (In Chinese with English abstract)
23. Xu, Y.X.; Hu, M.Y. Sedimentary provenance analysis of Oligocene Huagang Formation in Xihu Sag of East China Sea basin. *J. Oil Gas Technol.* **2010**, *5*, 176–179. (In Chinese with English abstract)
24. Hao, L.W.; Liu, C.; Wang, Q.; Wang, H.; Ma, X.F.; Tang, J.; Liao, P. Provenance characteristics of Huagang Formation (Paleogene) in Xihu Sag, East China Sea. *Nat. Gas Geosci.* **2011**, *22*, 9. (In Chinese with English abstract)
25. Wang, Z.Y. On marine to non-marine facies transformation of the Permian sedimentation in the Chaohu Lake, Anhui Province, with the application of MNO/TIO_2 index. *Pet. Geol. Exp.* **1992**, *14*, 195–199. (In Chinese with English abstract)
26. Xu, H.; Zhang, L.; Li, X.Q. *Geology and Hydrocarbon-Gas Hydrate Accumulation Dynamics in Shelf Basins in the East China Sea*; Science Press: Beijing, China, 2022; pp. 1–164. (In Chinese with English abstract)
27. Hall, J.; Wardle, R.J.; Gower, C.F.; Kerr, A.; Coflin, K.; Keen, C.E.; Carroll, P. Proterozoic orogens of the northeastern Canadian Shield: New information from the Lithoprobe ECSOOT crustal reflection seismic survey. *Can. J. Earth Sci.* **1995**, *32*, 1119–1131. [CrossRef]
28. Ren, J.J.; LI, S.T. Spreading and dynamic setting of marginal basins of the western Pacific. *Geosci. Front.* **2000**, *7*, 203–214. (In Chinese with English abstract)
29. Maruyama, S.; Isozaki, Y.; Kimura, G.; Terabayashi, M. Paleogeographic maps of the Japanese Islands: Plate tectonic synthesis from 750 Ma to the present. *Isl. Arc* **1997**, *6*, 121–142. [CrossRef]
30. Zhou, Z.Y.; Liao, Z.T.; Yang, F.L.; Fu, Q. Fission-track analysis and its application in the study of sedimentary basins. *Pet. Geol. Exp.* **2001**, *23*, 332–337. (In Chinese with English abstract)
31. Yang, F.; Yu, H.; Zhang, Q.; Li, Q. Correlations Between Shortening Rate, Uplift Rate, and Inversion Rate in Central Inversion Zone of Xihu Depression, East China Sea Basin. *J. Earth Sci.* **2009**, *20*, 699–708. [CrossRef]
32. Yang, C.H.; Wang, Y.M.; Lan, Z.; Wan, L.F.; Li, K.; Zhou, X.H. Delimitation of Cenozoic Rift-Depression Transitional Unconformity in Xihu Depression, East China Sea Shelf Basin. *Mar. Orig. Pet. Geol.* **2014**, *19*, 18–26.

Disclaimer/Publisher's Note: The statements, opinions and data contained in all publications are solely those of the individual author(s) and contributor(s) and not of MDPI and/or the editor(s). MDPI and/or the editor(s) disclaim responsibility for any injury to people or property resulting from any ideas, methods, instructions or products referred to in the content.